Unsupervised Segmentation of Synthetic Aperture Radar Inundation Imagery Using the Level Set Method

Ponlapak Phuhinkong*,Teerasit Kasetkasem†
*†Department of Electrical Engineering
Kasetsart University
Bangkok, Thailand
Emails: ponlapak.otto@hotmail.com*
fengtsk@ku.ac.th†

Preesan Rakwatin‡
‡GISTDA
The Government Complex
Bangkok , Thailand
Email: preesan@gistda.or.th‡

Thitiporn Chanwimaluang§
§Knowledge Elicitation and
Archiving Lab Laboratory,
NECTEC
Pathumthani, Thailand
Email: thitiporn.chanwimaluang@nectec.or.th§

Itsuo Kumazawa¶
¶Imaging Science and Engineering Laboratory
Tokyo Institute of Technology
R2-59, 4266 Nagatsuta-cho, Midori-ku
Yokohama, Japan
Email: kumazawa@isl.titech.ac.jp¶

***Abstract*—In this paper, we proposed an unsupervised algorithm to identify the flooded areas from synthetic aperture radar (SAR) images based on texture information derived from the gray-level co-occurrence matrices (GLCM) texture analysis. Here, five GLCM features, namely, energy, contrast, homogeneity, correlation and entropy, are extracted from a SAR image. These features are input to an image segmentation algorithm using a level set method to identify flooded and dry areas. Experiments were conducted on the RADARSAT-2 images of severely flooded areas near Chaopraya rivers, Thailand, in 2011, for which contemporaneous ground data exists for validation. Our results demonstrate that the proposed algorithm is able to successfully segment various flood regions and achieve improvement over existing published unsupervised algorithms.**

***Index Terms*—Flood detection, remote sensing, Level set, SAR, texture**

I. Introduction

Flood is one of the major disasters that occur worldwide. It has significant impacts on both human life and the economy. In Thailand, between August and December 2011, the severe flood occurred in the river networks in the central and the northern plains consisting of the Ping, Wang, Yom, Nan, Chao Phraya, Pasak and Chin rivers [1]. This flood areas covered 65 provinces and over 11 million rais (1.76 million hectors) on both urban and farming ares. 657 people were killed, 13 million people were evacuated from their homes, 4 million families lived without water and electricity for over three months, and about 19 billion bahts of government expenditure needed to be invested to repair the damage in the region. A major cause was the largest amount of rainfalls for over 70 years from five consecutive monsoon storms sweeping across Thailand.

After the flood, the Thai government allocated extra expenditure to mitigate and restore the flood-affected areas at the flat amount of around 20,000 bahts per home. This compensation was given to all flood-affected households regardless of severity of their damages. The more suitable approach for flood compensation is to subside the flood-affected households depending on the severity of the flood. One main factor to identify the severity of floods is the number of days that each flooded area is covered by water. In the past, the Thai government used the on-site inspection of damaged areas for the estimation of severity of the floods. However, due to the fact that the inundated areas, in 2011, were very wide and occurred over a long period, the inspection period took very long time and inaccurate. As a result, there is a need for the alternative approach that can quickly identify the flooded regions and determine the period of the flood. Remote sensing images due to their synoptic view and map-like format and the fact that some remote sensing satellites can take daily picture of earth surface enable the flood identification to be carried out on large areas in a timely fashion.

As result, it is reasonable to suggest that time series of radar and optical imagery can be used quantitatively in flood detection [1]. The automatic flood detection approach used in [1] may involve interpretation error due to the use of a simple threshold technique with real data. A survey on multi-temporal satellite data for flood assessment is presented [2] and [3]. This is valuable for the decision makers who plan the flood management measures. The utility of the flood spatial extent information is obtained from satellite sensors to calibrate and evaluate hydrological models in an effort to potentially improve hydrological prediction and flood management strategies in ungauged catchments [4].

In the absence of significant wind or rain, flooded areas would generally appear dark in optical image due to low reflectance of water in visible and infrared spectrum. However, floods are usually related to severe rain and heavy clouds. Hence, the flood identification with optical images is a very difficult task in practice since clouds can block sun-light and a direct view of the earth surface. An a result, many researchers focus on the use of the synthetic aperture radar (SAR) data such as the RADARSAT-2 in flood identification and monitoring. The major advantage of SAR sensor is the use of the microwave radiation rather than sun-light to produce an image. As a result, SAR images can be captured in all solar illumination and all weather conditions. In SAR imagery, backscatter depends on the surface roughness and the dielectric constant. Since the lands or non-water regions usually have a high dielectric constance, they will appear as the bright in SAR imageries. In contrast, open water regions appear dark due to the uneven surface which causes scattering in many directions. As a result, SAR images have recently received a great deal of attention in flooded area identification.

In [5], a statistical active contour model was employed to detect the flooded areas from the European Remote Sensing Satellite Synthetic Aperture Radar (ERS-1 SAR) images. Their results after comparing with aerial photography have shown to have a high accuracy in identification of the flooded areas of around 75%. Mason et al. [6] developed a flood detection system on urban areas using the TerraSAR-X images. The goal was to separate between showy pixels and watery pixels since reflectances from both pixels are quite similar and author reported that the accuracy was approximately 76% of the flooded areas. Schumann [7] found that multi-algorithm ensembles demonstrated with coinciding image acquisitions between different space-borne radar sensors to create a possibility of inundation maps. This causes high computation cost and inaccuracy if it uses unsuitable algorithms. In [8], authors used region-based level sets with the SAR data to identify water regions whose densities were estimated with the EM algorithm concurrently with the contour evolution. This method was very effective for image classification, but it was hampered by slow processing by using an EM algorithm with high computation cost.

Although the results from many research works are very promising. The overall accuracy is still limited since SAR images usually suffer from the speckle noises. A Speckle reduction filters [9] can be used to smooth out the speckle noise. However, these speckle noise filters tend to blur the boundaries between flood and no-flood regions. Furthermore, since the number of polarization in SAR image is limited, the water and non-water region can sometimes difficult to distinguish.

Hence, the objective of this study is to increase the accuracy of the flood region identification by incorporating texture information into the land cover mapping process. In this work, we employ the gray-level co-occurrence matrix (GLCM) to extract the texture information from the image and then apply the land cover mapping based on the level set method to classify an image into flood and non-flood regions. The texture characterizations used in our algorithm are the energy, contrast, correlation, homogeneity and entropy. The study used RADARSAT-2 images of severely flooded areas comparing with contemporaneous ground data existed for validation.

II. Background

Since our proposed algorithm uses the GLCMs to extract texture information from a SAR image, and employ the level set method to classify a SAR image into water and non-water regions, therefore, this section is devoted to provide a brief review of the GLCM and the level set method.

A. Texture Features Representation

Texture features is a very important in the human visual system. Experiments have demonstrated the ability of texture on the image segmentation [10] and have also demonstrated potential for classifying ice cover types in SAR imagery [11]. Several texture extraction methods in the research literature have been proposed such as Gabor filter [12] and Co-occurrence matrix [13]. In this paper, we focused on the gray-level co-occurrence matrices (GLCM) method due to its ability to characterize texture and its simplicity.

The GLCM method involves computing probabilities of all pairwise combinations of gray levels by assigning spatial window size and orientation. Moreover, gray-level quantization can reduce the effects of noise whereas texture information is reduced. In this paper, we employ five textural features in our study, namely, energy, contrast, correlation, homogeneity, and entropy since the texture information is created by the gray-level co-occurrence matrix of relative frequencies from a gray-scale image with two neighboring pixels in window size partitioned by the pixel distance D and angular. Denotes the horizontal and vertical length of the GLCM equal to the maximum gray level values in the specified window. Let $p(i,j)$ be the (i,j)th entry in the normalized GLCM. Each texture metrics are defined as follows:

Energy:

$$x_1 = \sum_i \sum_j p(i,j)^2 . \tag{1}$$

Contrast:

$$x_2 = \sum_i \sum_j (i-j)^2 P(i,j). \tag{2}$$

Correlation:

$$x_3 = \frac{\sum_i \sum_j (ij) p(i,j) - \mu_x \mu_y}{\sigma_x \sigma_y}. \tag{3}$$

Homogeneity:

$$x_4 = \sum_i \sum_j \frac{1}{1+(i-j)^2} p(i,j). \tag{4}$$

Entropy:

$$x_5 = -\sum_i \sum_j p(i,j) \log(p(i,j)). \tag{5}$$

where $\mu_x = \sum_i \sum_j i \cdot p(i,j)$, $\mu_y = \sum_i \sum_j j \cdot p(i,j)$, $\sigma_x = \sum_i \sum_j (i-\mu_x)^2 \cdot p(i,j)$ and $\sigma_y = \sum_i \sum_j (i-\mu_x)^2 \cdot p(i,j)$.

B. Level Set without Re-initialization

The general form of the level set formulation [14] is carried out by a curve C as the zero level set of the signed distance function of two dimensional level set function $\phi(t,(u,v))$, i.e., $C(t) = \{(u,v) \,|\phi(t,(u,v)) = 0\}$. In the image segmentation, the evolving level set without re-initialization function [15] as an approximate signed distance function during the evolution and the variational formulation defined by

$$E(\phi_k) = E_{int}(\phi_k) + E_{ext}(\phi_k), \tag{6}$$

where E_{int} and E_{ext} are the internal and external energies of the signed distance function. For the level set method without re-initialization, the internal energy is usually defined as

$$E_{int}(\phi_k) = \eta P(\phi_k) + \lambda L(\phi_k) + \nu_k A(\phi_k), \tag{7}$$

where η, λ and ν_k are parameters for controlling the each energy effects. The first term (internal energy) is a penalizing energy term that controls the deviation from the ideal signed distance function, the second term enforces the smoothness of the curve by reducing the length of the zero level set, and the third term provides different weight for different classes. With the above defined functions, the terms $P(\phi_k), L(\phi_k)$ and $A(\phi_k)$ are defined by

$$P(\phi_k) = \int_\Omega \frac{1}{2}\left(|\nabla\phi_k| - 1\right)^2 \mathrm{d}x\mathrm{d}y, \tag{8}$$

$$L(\phi_k) = \int_\Omega \delta(\phi_k)\,|\nabla\phi_k|\,\mathrm{d}x\mathrm{d}y, \tag{9}$$

and

$$A(\phi_k) = \int_\Omega H(\phi_k)\,\mathrm{d}x\mathrm{d}y. \tag{10}$$

where ∇ is the gradient operation, $H(\phi)$ is called the Heaviside function and used to distinguish the two classes and $\delta(\phi)$ is the impulse function that obtained by first derivative of the $H(\phi)$ defined as

$$H(\phi) = \begin{cases} 0 & ,\phi < 0 \\ 1 & ,\phi \geq 0 \end{cases} \tag{11}$$

In this paper, the Heaviside and impulse functions are approximated by

$$H_\epsilon(\phi) = \begin{cases} 1 & ,\phi > \varepsilon \\ 0 & ,\phi < -\varepsilon \\ \frac{1}{2}\left[1 + \frac{\phi}{\varepsilon} + \frac{1}{\pi}\sin\left(\frac{\phi\pi}{\varepsilon}\right)\right] & ,|\phi| \leq \varepsilon \end{cases} \tag{12}$$

and

$$\delta_\epsilon(\phi) = \begin{cases} 0 & ,|\phi| > -\varepsilon \\ \frac{1}{2\varepsilon}\left[1 + \cos\left(\frac{\phi\pi}{\varepsilon}\right)\right] & ,|\phi| \leq \varepsilon \end{cases} \tag{13}$$

to cope with sharp edges and infinity that cannot be realistically implemented where ϵ is a small positive constant.

In the level set, the goal is to determine the function $\phi(u,v)$ that minimizes the energy term, i.e., satisfying the Euler-Lagrange equation $\frac{\partial E}{\partial \phi} = 0$ [16]. The gradient flow that minimizes the functional E in [16], and denoted by

$$\frac{\partial \phi}{\partial t} = -\frac{\partial E}{\partial \phi}. \tag{14}$$

where $E = E_{int} + E_{ext}$. Here, E_{ext} is related to the observed SAR image.

III. Problem Statement

The label of classification map at pixel $s = (u,v)$ is denoted by $Y(s)$ which can also be computed the level set function and be represented two land cover class where $Y(s) \in \{0,1\}$ where 0 and 1 indicate water and non-water, respectively. Also, pixels inside and outside the closed contour of function $\phi(t,s)$ are indicated the Class $0(\Omega_0)$ for $\phi < 0$ and Class $1(\Omega_1)$ for $\phi > 0$, respectively. Hence, we represent the classification map is the function of $\phi(t,s)$ as

$$Y(s) = H(\phi(s)). \tag{15}$$

Since the flood map is a function of the level set function, hence, we apply the idea of the level set method proposed in [3], i.e.,

$$E = E_{int}(\phi) + E_{ext}(\phi). \tag{16}$$

The total energy function E depends on the value of ϕ and probability density function which consists of internal and external energies, respectively. We assume that the external energy depends on the GLCM features. In this paper, we adapt the multivariate normal distribution that is general enough to extract different types of image vector. Hence, the conditional probability density function (PDF) of feature vector $x_k(s)$ given the underlying land cover class is given by

$$Pr(x_k|y=i) = (2\pi)^{-\frac{K}{2}}\,|\Sigma_i|^{-\frac{1}{2}}\,e^{-\frac{1}{2}(x-\mu_i)^T\Sigma_i^{-1}(x-\mu_i)} \tag{17}$$

where μ_i and Σ_i are mean vector and covariance matrix derived from the GLCM feature image. The $(.)^T$ denotes the matrix transpose operation. Here, for the rest of the paper, we omit s for the sake of abbreviation. Here, the subscript i can be either 0 or 1 to indicate water and non-water classes, respectively. Hence, the external energy E_{ext} is defined as

$$E_{ext} = -\sum_{s\in S}\{l_0(x)\,H(\phi) + l_1(x)\,[1 - H(\phi)]\} \tag{18}$$

where $l_i(x) = \log Pr(x_k|y(s) = i)$, for $i = 0, 1$. The above summation can be approximated by the integration as

$$E_{ext} \approx -\int_\Omega E_x(u,v)\,\mathrm{d}u\mathrm{d}v \tag{19}$$

where
$E_x(u,v) = l_0(x(s_r))\,H(\phi(s)) + l_1(x(s_r))\,[1 - H(\phi(s))]$.
Here, s_r is the closet integer coordinate of (u,v).

IV. Proposed Algorithm

From Section III, the total energy function is obtained by following

$$E(\phi) = \eta P(\phi) + \lambda L(\phi) + \nu A(\phi) + \vartheta E_{ext} \quad (20)$$

Since ϕ is dynamic value function during evolution, the optimum solution can be obtained by minimizing the energy function. The derivative of E with respect to ϕ is given by

$$\frac{\partial E}{\partial \phi} = -\eta\left[\Delta\phi - div(\frac{\nabla\phi}{|\nabla\phi|})\right] - \eta\delta_\varepsilon(\phi)div(\frac{\nabla\phi}{|\nabla\phi|}) \quad (21)$$
$$-\nu\delta_\varepsilon(\phi) + \lambda\delta_\varepsilon(\phi)\left[l_0(x(s_r)) - l_1(x(s_r))\right]$$

where Δ is the Laplacian operator, div is the Divergence operator and $\delta_\varepsilon(\phi)$ is the approximation version of the impulse function.

The gradient flow is used to minimize the functional E in equation (21). Hence, the evolution of ϕ is fitting by the following motion partial differential equation as

$$\frac{\partial \phi}{\partial t} = \eta\left[\Delta\phi - div(\frac{\nabla\phi}{|\nabla\phi|})\right] + \eta\delta_\varepsilon(\phi)div(\frac{\nabla\phi}{|\nabla\phi|}) \quad (22)$$
$$+\nu\delta_\varepsilon(\phi) - \lambda\delta_\varepsilon(\phi)\left[l_0(x(s_r)) - l_1(x(s_r))\right]$$

Since the proposed algorithm is unsupervised, the initial flood map must be obtain from the observed SAR image without any supervision. Here, the k-mean algorithm is used to divide an image into five regions. Then, the automatic image thresholding method proposed by [17] is employed to divide these five regions into two groups. The groups of low and high intensity values are then assumed to be water and non-water, respectively. Next, the mean vectors and covariance matrices for water and non-water classes are estimated from the initial classified map. The proposed algorithm is then update l_0 and l_1. Next, the level set method in Eq. 22 to evolve the curve C, and an update flood map is obtaincd. Our proposed algorithm is then re-estimate mean vectors and covariance matrices from the updated flood map. This process is repeated until a convergence criteria is satisfied. The summary of the proposed algorithm is shown in Fig. 1.

V. Experimental Results

In all the experiments, the RADARSAT-2 medium-resolution single look complex images of the central plain in Thailand that covered flood regions which were acquired between July and December, 2011 were employed. All images were acquired in descending HH polarization mode. Our RADARSAT-2 data were acquired with variable incidence angles 42 degrees. The pixel size of products are 35.5 m × 55.5 m. We compiled five textural contexts based on GLCM method as input to our level set classification model. However, we could compare different accuracy between using and not textures in terms of classification power to demonstration that using textures can increase accuracy rate.

For preprocessing, we employ the k-means algorithm [18] to generate five clusters from the original SAR images. Further, we merge them into 2 classes, namely water and non-water

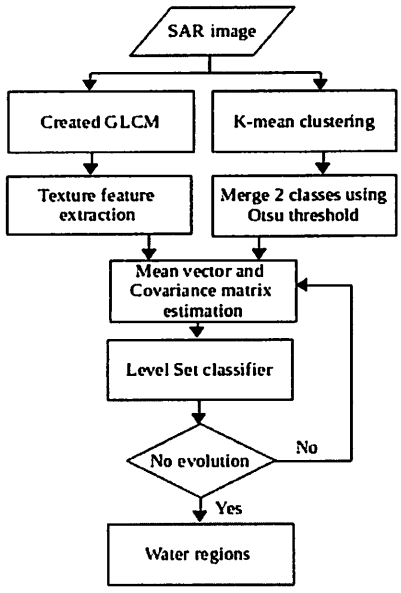

Fig. 1: The diagram of the proposed algorithm.

classes by using the Otsu thresholding method [17]. Next, the initial level set is obtained for water and non-water classes as the area inside and outside the contour, respectively. Next, we set the classification model parameters as follows: $\eta = 0.04, \lambda = 6, \nu_k = -1, \vartheta = 3, \rho = 6, \varepsilon = 1.5$ and time step $= 2$. To evaluate the performance of the proposed algorithm by comparing between the classified maps and the ground truth images, The authors adopt the confusion matrix approach [19] and Kappa Z-tests [20]. The Z-statistic was calculated as:

$$Z = \frac{\hat{k_1} - \hat{k_2}}{\sqrt{\frac{k(1-k)}{n}}} \quad (23)$$

where $\hat{k_1}, \hat{k_2}$ are the two Kappa values, and k is variance with n samples (choose $k = 0.5$ maximum variation). The null hypothesis is rejected if the Z-statistic is greater than the critical value (1.96 for a 95% confidence level).

To evaluate the performance of our proposed method, we compare our approach with other three image classification algorithms, namely, 1) the Otsu thresholding method [17], 2) the k-means clustering method [18] and 3) the level set without re-initialization technique [3] on a SAR image without texture feature extraction.

The first studied site (Fig. 2(a)) is at Sapphaya, Chainart around Chaopraya river. This area was flood during September 2011. Fig. 2(a) displays the observed RADARSAT-2 image on September 27th, 2011. The image shows flood water in open land, and the goal is to calculate the water concentration. The ground truth image of the homogeneous area is created by human observation, and show in Fig.2(b). The three methods are applied to segment this image based on intensity only. As the pixels of water and non-water are separable obviously in the intensity level, the Otsu threshold, the k-means clustering and the traditional level set method can properly separate

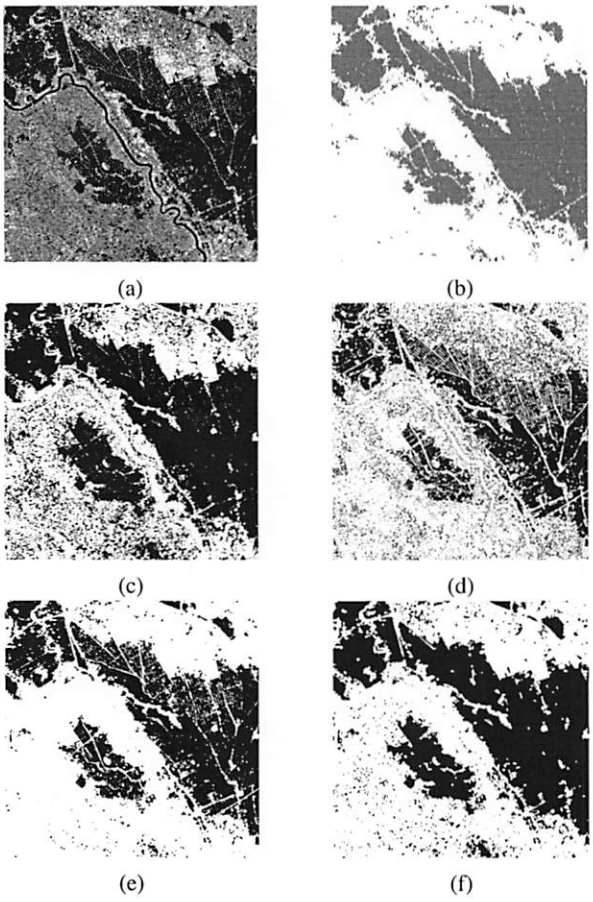

Fig. 2: (a) SAR flood image of Sapphaya, Chainart province. (b) the ground truth image (blue is water area). Intensity-based segmentation using (c) Otsu thresholding (86.31%), (d) k-means (76.87%), (e) the level set method on the intensity image [3] (88.97%) and (f) the proposed algorithm (91.69%).

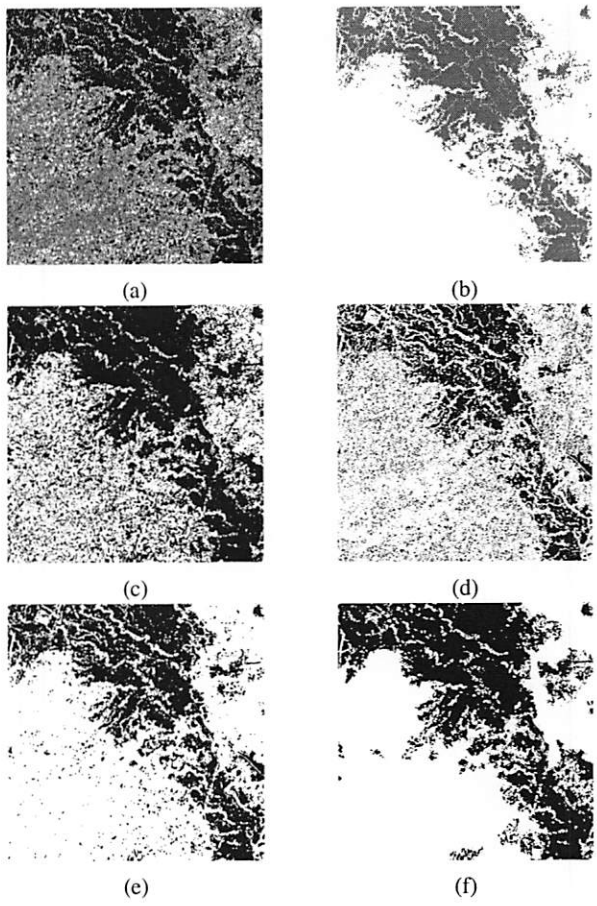

Fig. 3: (a) SAR flood image of Bangrakam, Phisanulok province. (b) the ground truth image (blue is water area). Intensity-based segmentation using (c) Otsu thresholding (79.88%), (d) k-means (79.47%), (e) the level set method [3] (90.91%) and (f) the proposed algorithm (91.84%).

water and non-water classes, as shown in Fig. 2(c), 2(d) and 2(e), respectively. Both the traditional level set method with intensity as a feature (Fig. 2(e)) and the level set method with including textures (Fig. 2(f)) improve the discrimination of in the water and non-water regions, generating effective segmentations. These examples illustrate the ability of the contour to automatically split since both water and non-water classes are disconnected. Moreover, our proposed method (Fig. 2(f)) indicates that the most successful segmentation approach comparison with three candidate techniques with the overall accuracy of 91.69% (2.72% better than Fig. 2(e))

The second studied site (Fig. 3(a)) is located fields in Bangrakam, Phisanulok where it has been flooded during the August 2011. Fig.3(b) shows the ground data of flood of rice fields on August 24th, 2011. From Fig 3(c), we observe that the intensity-based image thresholding cannot separate water from non-water regions. The automatic threshold method was able to segment the thick flood areas. However, it failed in the high speckle noise regions in the image. Like in Ostu algorithm, the k-mean clustering algorithm was unable to classify the image correctly in the high speckle noise area (Fig. 3(d)). Both proposed algorithm (Fig. 3(f)) and Phuhinkong's algorithm [3] (Fig. 3(e)) can increase the accuracy of the flood detection by incorporating the level set methods. Even though the proposed algorithm can achieve a slight improvement of 0.91%, our proposed algorithm is more robust to the speckle noise such as in the area on the low left region of the image. This result demonstrates that the texture information can reduce the effect of speckle noise in the flood identification.

To quantitatively assess the accuracy of the proposed algorithm in the study areas, the confusion matrices for all two studied sites are computed in Tables I. For all cases, the proposed algorithm were able to identify flooded and dry area with the accuracy of more than 85%. In fact, in the Phisanulok where a large area is contaminated by speckle noise, the accuracy is more than 90%. The users and producers accuracies for all two sites are also very high. Table II summarizes the Kappa Z-test statistics of the four classifications for comparing the optimal segmentation with the other segmentations. The highest classification Kappa of 0.83 was achieved by the

TABLE I: Statistics of algorithm performance

Site 1	Reference data		
Classified label	Flood	No flood	Producer's Accuracy (%)
Flood	747358	111922	86.97
No flood	43161	963074	96.71
User's Accuracy (%)	94.54	89.59	**91.69**
Kappa	0.831		
Site 2	Reference data		
Classified label	Flood	No flood	Producer's Accuracy (%)
Flood	1274452	138995	90.16
No flood	157485	2063468	92.90
User's Accuracy (%)	89.0	93.69	**91.84**
Kappa	0.829		
Overall Accuracy : 91.77%			

TABLE II: Kappa Z-test statistics for two sites at $H_0 : k_i = k_j (i \neq j)$ when k is the Kappa value. Values in bold indicate significant difference between the two classifications on a 95% confidence level. OT:Otsu thresholding; KM:K-Means; LSM:Level Set Method; TLSM:Texture-based Level Set Method.

Site 1					
Classification	OT	KM	LSM	TLSM	Kappa
OT	N/A				0.727
KM	**546.33**	N/A			0.527
LSM	**128.38**	**674.72**	N/A		0.774
TLSM	**284.09**	**830.43**	**155.70**	N/A	0.831
Site 2					
Classification	OT	KM	LSM	TLSM	Kappa
OT	N/A				0.607
KM	**205.89**	N/A			0.553
LSM	**747.31**	**953.20**	N/A		0.803
TLSM	**846.44**	**1052.33**	**99.13**	N/A	0.829

texture-based segmentation using level set method significantly better than the other segmentation.

VI. Conclusion

In this paper, a new method for an automatic flood identification is proposed, developed, and tested successfully for the SAR images. Published methods such as Otsu thresholding and k-means clustering cannot accurately detect floods in SAR images due the presence of the speckle noises. To address this problem, we have proposed a new algorithm that extracts the texture features from a SAR image and couples with the level set method to classify a SAR image into water and no-water regions. We have demonstrated the performance of the proposed algorithm is superior to other algorithms in two flooded areas in Thailand. In future research a method for automated determination of optimal parameters in the proposed algorithm needs to be studied. Also, the computational times of all methods should be compared. The automation of classification is necessary and worthy for flood identification of further study.

Acknowledgment

The authors wish to express their gratitude towards Geo-Informatics and Space Technology Development Agency (GISTDA) for providing the ground truth data. This research work is also supported in part by Thailand Advanced Institute of Science and Technology (TAIST), National Science and Technology Development Agency (NSTDA), Tokyo Tech Institute of Technology and Kasetsart University (KU).

References

[1] K. Auynirundronkool, N. Chen, C. Peng, C. Yang, J. Gong, and C. Silapathong, "Flood detection and mapping of the thailand central plain using radarsat and modis under a sensor web environment," *International Journal of Applied Earth Observation and Geoinformation*, vol. 14, pp. 245–255, 2012.

[2] J. Senthilnath, S. Omkar, V. Mani, and P. Diwakar, "Multi-temporal satellite imagery for flood damage assessment," *Journal of the Indian Institute of Science*, vol. 93, pp. 105–115, 2013.

[3] P. Phuhinkong, T. Kasetkasem, P. Rakwatin, T. Chanwimaluang, and I. Kumazawa, "Inundation region identification using the level set method," *The International Conference of Information and Communication Technology for Embedded Systems*, January 2014.

[4] S. I. Khan, Y. Hong, J. Wang, K. K. Yilmaz, J. J. Gourley, R. F. Adler, G. R. Brakenridge, F. Policelli, S. Habib, , and D. Irwin, "Satellite remote sensing and hydrologic modeling for flood inundation mapping in lake victoria basin: Implications for hydrologic prediction in ungauged basins," *IEEE transaction on geoscience and remote sensing*, vol. 49, no. 1, pp. 85–95, January 2011.

[5] M. S. Horritt, D. C. Mason, and A. J. Luckman, "Flood boundary delineation from synthetic aperture radar imagery using a statistical active contour model," *International Journal of Remote Sensing*, vol. 22, no. 13, pp. 2489–2507, August 2001.

[6] D. C. Mason, R. Speck, B. Devereux, G. Schumann, J. C. Neal, and P. D. Bates, "Flood detection in urban areas using terrasar-x," *IEEE transactions on geoscience and remote sensing*, vol. 48, no. 2, pp. 882–894, February 2010.

[7] G. Schumann, G. D. Baldassarre, and P. D. Bates, "The utility of spaceborne radar to render flood inundation maps based on multialgorithm ensembles," *IEEE transactions on geoscience and remote sensing*, vol. 47, no. 8, pp. 2801–2807, September 2009.

[8] M. Silveira and S. Heleno, "Separation between water and land in sar images using region-based level sets," *IEEE geoscience and remote sensing letters*, vol. 6, no. 3, pp. 8–37, July 2009.

[9] A. Lopes, E. Nezry, R. Touzi, and H. Laur, "Structure detection and statistical adaptive speckle filtering in sar images," *International Journal of Remote Sensing*, vol. 14, pp. 1735–1758, 1993.

[10] C. H. Chen, L. F. Pau, and P. S. P. Wang, "Texture analysis," *The Handbook of Pattern Recognition and Computer Vision (2nd Edition)*, pp. 207–248, 1998.

[11] H. Deng and D. A. Clausi, "Unsupervised segmentation of synthetic aperture radar sea ice imagery using a novel markov random field model," *IEEE Transactions on Geoscience and Remote Sensing*, vol. 43, pp. 528–537, March 2005.

[12] J. Daugman, "Complete discrete 2-d gabor transforms by neural networks for image analysis and compression," *IEEE Trans on Acoustics, Speech, and Signal Processing*, vol. 36, pp. 1169–1179, July 1988.

[13] R. M. Haralick, K. Shanmugam, and I. Dinstein, "Textural features for image classification," *IEEE Transactions on Systems, Man, and Cybernetics*, vol. 6, pp. 610–621, 1973.

[14] S. Osher and J. A. Sethian, "Fronts propagating with curvaturedependent speed: algorithms based on hamilton-jacobi formulations," *Journal of Computational Physics*, vol. 79, pp. 12–49, 1988.

[15] C. Li, C. Xu, C. Gui, and M. D. Fox, "Level set evolutionwithout reinitialization: A new variational formulation," *IEEE Computer Society Conference on Computer Vision and Pattern Recognition*, no. 8, pp. 1063–6919, 2005.

[16] G. Aubert and P. Kornprobst, "Mathematical problems in image processing: Partial differential equations and the calculus of variations," *New York: Springer-Verlag*, 2002.

[17] N. Otsu, "A threshold selection method from gray-level histograms," vol. 9, pp. 62–66, 1979.

[18] Arthur and S. Vassilvitskii, "k-means++: the advantages of careful seeding," *Proceedings of the eighteenth annual ACM-SIAM symposium on Discrete algorithms*, 2007.

[19] S. V. Stehman, "Selecting and interpreting measures of thematic classification accuracy," *Remote Sensing of Environment*, vol. 62, pp. 77–89, 1997.

[20] R. G. Congalton and K. Green, *Assessing the Accuracy of Remotely Sensed Data: Principles and Practices*, 2008.